Universiteit
Leiden
The Netherlands

Unravelling vascular tumors : combining molecular and computational biology

IJzendoorn, D.G.P. van

Citation
IJzendoorn, D. G. P. van. (2020, January 16). *Unravelling vascular tumors : combining molecular and computational biology*. Retrieved from https://hdl.handle.net/1887/82754

Version:	Publisher's Version
License:	Licence agreement concerning inclusion of doctoral thesis in the Institutional Repository of the University of Leiden
Downloaded from:	https://hdl.handle.net/1887/82754

Note: To cite this publication please use the final published version (if applicable).

Cover Page

Universiteit Leiden

The handle http://hdl.handle.net/1887/82754 holds various files of this Leiden University dissertation.

Author: IJzendoorn, D.G.P. van
Title: Unravelling vascular tumors : combining molecular and computational biology
Issue Date: 2020-01-16

Chapter 6

Pseudomyogenic hemangioendothelioma recapitulated in endothelial cells from human induced pluripotent stem cells engineered to express the *SERPINE1-FOSB* translocation

This chapter is based on the manuscript: **van IJzendoorn DGP**, Salvatori DCF, Cao X, van den Hil F, Briaire-de Bruijn IH, de Jong D, Mei H, Mummery CL, Szuhai K, Bovée JVMG, Orlova VV. Pseudomyogenic hemangioendothelioma recapitulated in endothelial cells from human induced pluripotent stem cells engineered to express the *SERPINE1-FOSB* translocation.

6.1 Abstract

Chromosomal translocations are prevalent among soft tissue tumors including those of the vasculature. Pseudomyogenic hemangioendothelioma (PHE) is one such tumor. It has features of endothelial cells (ECs) and a tumor-specific t(7;19)(q22;q13) *SERPINE1-FOSB* translocation, but has been difficult to study since to date no cell lines have been derived from the tumor. To address this, we engineered the PHE chromosomal translocation into human induced pluripotent stem cells (hiPSCs) using CRISPR/Cas9 and differentiated these into ECs (hiPSC-ECs). Comparison of parental and modified (PHE) lines with the t(7;19)(q22;q13) *SERPINE1-FOSB* translocation showed (i) elevated expression of *FOSB* specifically in hiPSC-ECs *in vitro* and *in vivo* (ii) increased proliferation and tube formation but decreased endothelial barrier function (iii) invasive growth and abnormal vessel formation in mouse after transplantation of the mutated cells (iv) transcriptome alterations specific for hiPSC-ECs that reflect the PHE phenotype and elucidate pathways regulated by the fusion that can be targeted for treatment (PI3K-Akt and MAPK signaling). hiPSC-ECs carrying the *SERPINE1-FOSB* translocation thus recapitulated functional features of PHE and demonstrated that this approach can yield models of translocation-driven tumors for identification of therapeutic targets and deeper understanding of underlying tumorigenic mechanisms.

6.2 Introduction

Chromosomal translocations and their corresponding gene fusions are common in neoplasia and are important in the initiation of tumorigenesis (1). These gene fusions are especially prevalent in soft tissue tumors, of which ∼15-20% carry a recurrent chromosomal translocation with no, or few, additional genomic alterations (2). Moreover, translocations are usually specific for each subtype. The identification of specific fusion genes has significantly increased the understanding of the pathogenesis of these (often-rare) tumor types and are used as an auxiliary diagnostic tool.

Pseudomyogenic hemangioendothelioma (PHE) is a rare soft tissue tumor characterized by a specific recurrent balanced translocation, t(7;19)(q22;q13), which fuses *SERPINE1* to *FOSB* (3, 4). The translocation leads to the loss of the first exon of *FOSB* containing the start codon, resulting in a novel start codon in exon 2 of *FOSB*. The translocation therefore causes loss of 48 amino acids at the start of the FOSB protein which then falls consequently under control of the *SERPINE1* promoter (4). PHE is locally aggressive, rarely metastasizing and often affecting young adults, especially men between 20-50 years of age. The disease most often presents as multiple discontiguous lesions in different tissue planes (5). Approximately 60% of the patients show relapse after surgical removal

or develop additional nodules which can necessitate limb amputation. The tumors display loose spindle-shaped cells with abundant eosinophilic cytoplasm, that invade in the surrounding soft tissues, expressing vascular (CD31, ERG) and epithelial (keratin) markers. Moreover, the translocation results in overexpression of FOSB protein in patient tumor samples (6). Although PHE does not form functional blood vessels, vascular markers are expressed suggesting that PHE arises from endothelial cells (ECs) or their precursors. The tumor is therefore classified among the group of vascular tumors (5, 7, 8).

Like many other soft tissue tumors with translocations, PHE is rare and no cell lines have yet been derived from the tumor, confounding understanding of tumorigenesis and the identification of potential therapeutic targets. A possible approach to model translocation driven tumors is to engineer the complete chromosomal translocation in human pluripotent stem cells and examine the effects on appropriately differentiated derivatives (9). Engineered nucleases were recently shown to be useful in generating chromosomal translocations in human cells. Clustered regularly interspaced short palindromic repeats (CRISPR) and Cas9 nucleases have been used to introduce chromosomal translocations in human umbilical cord-derived mesenchymal stromal cells (hMSCs), umbilical cord blood-derived CD34+ cells, and more recently human induced pluripotent stem cells (hiPSCs) (10–13). hiPSCs in particular are increasingly used as human disease models, as they can be propagated indefinitely *in vitro* and differentiated into most cell types of the body (14), including ECs (15–17). They are thus a renewable source of cells to study human physiology and disease. We hypothesized that hiPSC-derived ECs (hiPSC-ECs) could be valuable for modeling rare tumors such as those of the vasculature and demonstrated in the study described here that this is indeed the case for PHE.

We introduced the t(7;19)(q22;q13) *SERPINE1-FOSB* translocation into hiPSCs and thus generated control and modified isogenic hiPSC pairs. We carried out functional analysis of hiPSC-ECs and whole genome and transcriptome sequencing of isogenic pairs of hiPSC and hiPSC-EC with and without translocation. We showed that hiPSC-ECs with the *SERPINE1-FOSB* fusion were distinct from their isogenic controls and exhibited phenotypic and transcriptomic characteristics very similar to PHE. More importantly, in mice mutant hiPSC-ECs became invasive and formed abnormal vessels. Our hiPSC model thus mimics PHE, but in more general terms, the approach can serve as a blueprint for using CRISPR/Cas9 in hiPSCs to explore the role of fusion genes in the development of specific rare cancer subtypes for which cell lines are lacking, providing deeper understanding of tumorigenesis resulting from gene fusions.

6.3 Materials and Methods

6.3.1 hiPSC lines and culture

The SeV reprogrammed hiPSC line LUMC0054iCTRL was used (additional information available in public databases: `http://hpscreg.eu/cell-line/LUMCi001-A` and `http://hpscreg.eu/cell-line/LUMCi001-A-1`) (15). hiPSCs were cultured on recombinant vitronectin (VN)-coated plates in TeSR-E8 all from STEMCELL Technologies (SCT), according to the manufacturer's instructions. For targeting experiments, hiPSCs were adapted to single cell passaging on mouse embryonic fibroblasts (MEFs) in Dulbecco's modified Eagle's medium/Ham's F-12 medium (DMEM/F12) supplemented with 20% knockout serum replacement (Invitrogen), 1 mM L-glutamine, 0.1 mM nonessential amino acids, 0.1 mM 2-mercaptoethanol, and 8 ng/ml recombinant human basic fibroblast growth factor (bFGF; Milteny). Single cell adapted hiPSC were passaged using 1X TrypLE Select with additional supplementation with 1X RevitaCell (Invitrogen).

6.3.2 Construction of dual-guide Cas9-encoding plasmids and repair template

A dual sgRNA and Cas9-expressing plasmid was generated by introducing a second gRNA scaffold in the SpCas9-2A-Puro V2.0 (Addgene, Feng Zang) plasmid using Gibson ligation as described (18). The final plasmid contains *FOSB* sgRNA TCCACTACACCGTGACGCAG and *SERPINE1* sgRNA TGAACACTAGGGCAAGGTGC. The repair template was generated by blunt ligation of *FOSB* and *SERPINE1* homology arms (around 1kb each) into a P15 backbone containing a Neomycin resistance cassette surrounded by two flippase recognition target (FRT) sequences (kindly provided by Dr. Konstantinos Anastassiadis, Technical University Dresden). The CAGGs-Flpo-IRES-puro vector which expresses codon-optimized Flp recombinase was used for transient transfection to recombine FRT sites (19) (kind gift of Dr Konstantinos Anastassiadis). The U6 vector used for the Gibson ligation was a kind gift from Dr. Andrea Ventura (Addgene plasmid # 69312).

6.3.3 Transfection

hiPSCs were transfected at 60-70% confluence the day after seeding in a 60 mm dish. Transfection was carried out using Lipofectamine 2000 (Invitrogen). First, 20 μl Lipofectamine 2000 was diluted in 300 μl Opti-MEM Medium and incubated at RT for 5 min. In parallel, 8 μg of both the repair template and double guide RNA/Cas9 was diluted in 300 μl Opti-MEM Medium. Diluted plasmid DNA was added to diluted Lipofectamine 2000 in

a 1:1 ratio and incubated another 5 min at RT before the DNA-lipid complex was added to the cells in a drop-wise manner. Cells were allowed to grow in the incubator for ∼18 hours before the medium was changed. Antibiotic selection with 50 μg/ml G-418 was performed 24 hours post transfection and was continued for 7 days to select for targeted cells. Once recovered, cells were passaged into 6-well plates and transfected the next day with 4 μg Flp recombinase expression vector to excise the neomycin cassette (using Lipofectamine 2000, according to the manufacturer's protocol). At 24h post transfection the medium was supplemented with 0.5 μg/ml Puromycin for 48h to enrich for transfected cells. At 80% confluence, the cells were passaged for clonal expansion on 96-well plates using limited dilution.

6.3.4 Fluorescence In Situ Hybridization

Three-color Fluorescence In Situ Hybridization (FISH) was performed using BAC clones (BACPAC Resource Center). Proximal to *SERPINE1* BAC clone RP11-395B7 was selected. Proximal and distal to *FOSB* respectively BAC clone RP11-84C16 and RP11-902P17 were selected. BAC DNA was extracted using the High Pure plasmid isolation kit (Roche). The RP11-395B7, RP11-84C16 and RP11-902P17 were respectively labeled with Cy5-dUTP, Fluorescein-12-dCTP and Cy3-dUTP using a nick translation labeling reaction (20). FISH was performed as previously described by our group (21). Representative images were taken using a fluorescence microscope (Leica).

6.3.5 Identification of targeted hiPSC clones by PCR

PCR screening was performed to determine the presence of both the 5' homology arm of *SERPINE1* (primers SF and FR), the 3' homology arm of *FOSB* (primer F2 and R2), the wild-type *SERPINE1* (primer SF and SR) and wild-type *FOSB* (primer FF and FR) in clonal lines (table 6.1). Colonies were picked in maximum 2 μl hESC-food and added to 20 μl QuickExtract Solution (Epicentre) in 0.5 mL tubes. The tubes were vortexed for 15s and DNA was extracted by heating the samples to 65 °C for 15 minutes, 68 °C for 15 minutes and 98 °C for 10 minutes in a thermocycler. 2-Step PCR was performed with Terra PCR Direct Polymerase (TaKaRa) according to the manufacturer's protocol. Sanger sequencing was performed (BaseClear) to confirm the *SERPINE1-FOSB* fusion and to screen the *SERPINE1* and *FOSB* wild-type allele for on-target mutations due to NHEJ.

Name	Sequence
SERPINE1 (SF)	ACACAGGCAGAGGGCAGAAAGGTCAA
SERPINE1 (SR)	CCTGCGCCACCTGCTGAAACAC
FOSB (FF)	GCCTTCAGAGCAGTTCCAGGAGTCCATTTA
FOSB (FR)	ACCGACACACACACACCCAACACACATAA
F2	TGGGCTGCAAAGGCAGAGAGTGGTAAT
R2	AAGCGATCCTCCCACTAAAGCCTCCATAGT

Table 6.1: PCR primers used to screen targeted clones.

6.3.6 COBRA-FISH

COmbined Binary RAtio Fluorescence in Situ Hybridization (COBRA-FISH) was performed on metaphase cells as previously described in detail (22, 23).

6.3.7 Differentiation and characterization of hiPSCs to ECs

hiPSCs were differentiated to hiPSC-ECs and characterized as previously described (15–17).

6.3.8 Real-Time qPCR

RNA isolation was performed with the Direct-zol RNA isolation kit (Zymo-research) according to the manufacturer's protocol. cDNA was synthesized using M-MLV with oligo dT primers (Promega) according to the manufacturer's protocol. Real-Time qPCR was performed with Sybr Green (Bio-Rad) on a CFX384 thermocycler (Bio-Rad). All real time PCR experiments were performed in triplicate. Primers are listed in table 6.2.

Name	Sequence
HPRT_f	TGACACTGGCAAAACAATGCA
HPRT_r	GGTCCTTTTCACCAGCAAGCT
FOSB_f	AGCAGCAGCTAAATGCAGGA
FOSB_r	CCAACTGATCTGTCTCCGCC

Table 6.2: qPCR primers.

6.3.9 Western blotting

Western blotting was performed as previously described (24) using FOSB monoclonal rabbit antibody (#2251; Cell Signaling) and USP7 monoclonal rabbit antibody (A300-033A; Bethyl).

6.3.10 Assessment of hiPSC-EC proliferation

To quantify proliferation, cells were cultured in a 96-well plate for 24 hours. Presto Blue (ThermoFisher) was subsequently added to the medium and cells were incubated at 37 °C for 30 minutes before determining the Relative Fluorescence Units (RFU) using a plate reader (Perkin Elmer).

6.3.11 Matrigel tube formation assay

Tube formation assays were performed in 96-well plates coated with 50 μl Matrigel (Corning). hiPSC-ECs were seeded at a density of 15,000 cells per well in 150 μl EC-SFM supplemented with 1% BSA and 50 ng/μl VEGF. Tube formation was analyzed with ImageJ (NHI, v1.51s). Tube formation was imaged with the EVOS Cell Imaging System (ThermoFisher). To quantify tube formation a custom plugin in ImageJ (NIH, v1.51s) was used. Analysis scripts are available on GitHub (`github.com/davidvi`) for analysis of tube formation.

6.3.12 Endothelial barrier function and analysis

Endothelial barrier function was determined as previously described (15). Briefly, hiPSC-ECs were plated on FN-coated ECIS arrays (8W10E PET, Applied Biophysics) at a density of 50,000 cells/cm2. Wounding of the cells grown on the electrodes was performed by applying a 10 sec pulse of 5V at 60 kHz. Barrier function was estimated by applying a current to the electrodes at 4 kHz and measuring the R [ohm]. Barrier function was measured for over 8 hours. Quantification was performed over a period of 5 hours, when the barrier had stabilized.

6.3.13 Immunohistochemistry

Immunofluorescence was performed as previously described (15, 16). Briefly, hiPSC-ECs were fixed with 4% PFA and permeabilized with 0.1% Triton-X100. The following primary antibodies were used: anti-ZO1 (61-7300; ThermoFisher), VEC (53-1449-42; CellSignaling), CD31 (M082301; Dako) and cells were counterstained with A488 conjugated Phalloidin (ThermoFisher). Incubation with primary antibodies was overnight at +4 °C and secondary antibodies for 30 minutes at room temperature. Immunohistochemistry with human-specific CD31 (huCD31) and FOSB was performed as previously described (15). Images were acquired using EVOS FL AUTO2 Imaging System (ThermoFisher) or with the WLL1 confocal microscope (Leica), using 40x DRY objective and 0.75 Zoom factor. Used Antibodies are listed (table 6.3).

Antibody	Cat#	Manufacturer	Clone	Dilutions
VE-cadherin-A488	53-1449-42	eBiosciences	16B1	1:100
KDR-PE	FAB357P	R&D systems	89106	1:50
VEGFR3-PE	FAB3492P	R&D systems	54733	1:50
CD31-APC	17-0319-42	eBiosciences	WM59	1:200
CD34- PerCP-Cy5.5	347222	BD Pharmingen	8G12	1:100
CD105-VioBlue	130-099-666	Miltenyi Biotec	43A4E1	1:50
Phalloidin-A488	A12379	ThermoFisher	N/A	1:20
VE-Cadherin	2158S	Cell Signaling	Polyclonal	1:200
ZO-1	61-7300	ThermoFisher	Polyclonal	1:200
CD31	M0823	Dako	JC70A	1:200 IF 1:30 IHC
FOSB	2251S	Cell Signaling	5G4	1:200 IF 1:30000 WB
USP7	A300-033A	Bethyl Laboratories	Polyclonal	1:10000

Table 6.3: Antibodies and their dilutions.

6.3.14 Vasculogenesis *in vivo* in mice

All animal experiments were performed in accordance with legal regulations with approved protocols by the Central Commissie voor Dierproeven (CCD, Central Commission for Animal Experiments). Mice were maintained at the animal facility of Leiden University Medical Center (LUMC). Teratoma and Matrigel plug assays (figure 6.5a) were performed in eight week old male NSG mice (NOD.Cg-Prkdcscid Il2rgtm1Wjl/SzJ, Charles River).

6.3.15 Teratoma assay

The teratoma assay was performed on the parental hiPSC^{WT} and hiPSC$^{SERPINE\text{-}FOSB(D3)}$ as reported before (25). On the same day, three animals per cell-line were injected using the same batch of cells for each mouse.

6.3.16 *In vivo* mouse Matrigel plug assay

The Matrigel plug assay was performed as described previously (15, 26). Plugs were removed after 4 and 16 weeks. For each time points three mice were injected with hiPSC^{WT} and three mice with hiPSC$^{SERPINE\text{-}FOSB(D3)}$ (figure 6.5a). Each mouse was subcutaneously injected in the right and left flank with a mixture of hiPSC-ECs, human bone marrow-derived stromal cells (BMSCs) (PromoCell) and Matrigel (Corning). Vessel density was estimated by quantifying the human CD31+ area in serial sections as described previously (15).

6.3.17 Phosphotungstic acid-haematoxylin staining and analysis

PTAH staining was performed on 4 μm FFPE sections. Paraffin was removed with xylene and sections were rehydrated in an ethanol gradient. Sections were incubated for 15 minutes in 0.25% potassium permanganate then 5 minutes in 5% oxalic acid. Last, the sections were incubated for 24 hours in PTAH solution. To analyze thrombus formation in vessels all vessels with fibrin were counted in an area of 5.7 mm^2.

6.3.18 Whole genome and transcriptome sequencing and analysis

DNA was isolated for whole genome sequencing using the Wizard Genomic DNA Purification Kit (Promega) and sequenced on the BGISEQ-500 platform (BGI). Reads were aligned to the GRCh38/hg19 reference genome using the Burrow-Wheeler Aligner (v0.7.12) and further processed according to the GATK (Broad institute) best practice pipeline. Copy Number Analysis (CNA) was performed using VarScan (v2.2.4) and analyzed using DNAcopy R package (v3.6). Off-target sites for the used gRNAs were determined using an online tool (`crispr.cos.uni-heidelberg.de`). Data was visualized with the circlize R package (v0.4.3). RNA for transcriptome sequencing was isolated using Direct-zol RNA miniprep kit (Zymo Research). After library preparation, sequencing was performed on the BGISEQ-500 platform (BGI). Raw data was processed using the LUMC BIOPET Gentrap pipeline (`https://github.com/biopet/biopet`), which comprises FASTQ preprocessing, alignment and read quantification. Sickle (v1.2) was used to trim low-quality read ends15. Cutadapt (v1.1) was used for adapter clipping16, reads were aligned to the human reference genome GRCh38 using GSNAP (gmap-2014-12-23) (27, 28) and gene read quantification with htseq-count (v0.6.1p1) against the Ensembl v94. Gene length and GC content bias were normalized using the R package cqn (v1.28.1) (29). Genes were excluded if the number of reads was below 5 reads in $\leq$90% of the samples. The final dataset comprised gene expression levels of 6 samples and 16,510 genes. Differentially expressed genes were identified using generalized linear models as implemented in (30). P-values were adjusted using the Benjamini-Hochberg procedure and PFDR ≤ 0.05 was considered significant. Normalized RPKM values were log2 transformed and standardized across each gene using z-scores and heatmap was produced with the R package ggplot2 (v2.2.1). KEGG pathway enrichment analysis was carried out using Enrichr (31, 32) computational tool and $q < 0.05$ was used as the cutoff for significant pathways. Gene ontology (GO) enrichment analysis and cnetplot of selected GOs were done with R package clusterProfiler (v3.10.1) (33), $q < 0.05$ was used as the cutoff for significant GOs. Interaction networks of input genes were predicated using Interaction network analysis function of Ingenuity Pathway Analysis (IPA) software. Then, interac-

tions between specific genes and selected networks were generated using the Build function of IPA.

6.3.19 Statistical Analysis

Statistics and graphs for real-time PCR, proliferation, tube formation and barrier function were generated with GraphPad Prism (GraphPad Software). One-way ANOVA with Tukey's multiple comparison for the analysis of three or more groups or Mann-Whitney test for analysis of two groups were used. The data are reported as mean ±SD.

6.3.20 Data availability

Whole-genome and transcriptome sequencing data was deposited to the Sequence Read Archive under accession PRJNA448372.

6.4 Results

6.4.1 Introduction of t(7;19)(q22;q13) *SERPINE1-FOSB* translocation in hiPSCs

We used CRISPR/Cas9-facilitated gene targeting to introduce the t(7;19)(q22;q13) translocation in hiPSCs. We generated a fusion between intron 1 of *SERPINE1* and intron 1 of *FOSB*, which leads to the same novel start codon as found in PHE tumors from patients (figure 6.1a). Two double stranded DNA breaks were introduced in the genome guided by two gRNAs targeting *SERPINE1* intron 1 and *FOSB* intron 1. A repair template was provided for homologous directed recombination (HDR) containing two 1000 bp homology arms for *SERPINE1* and *FOSB*, separated by an excisable neomycin resistance cassette flanked by Flp-recombinase sequences (FRT) (figure 6.1a). A wild-type hiPSC line generated from an anonymous "healthy" donor using non-integrating Sendai virus (SeV) was used for targeting (15). hiPSCs were simultaneously transfected with vectors containing Cas9, gRNAs and HDR template (schematic overview of the targeting strategy in hiPSCs is shown in supplementary figure 6.1a). Neomycin selection allowed enrichment of hiPSCs with integration of the targeting template. The neomycin cassette was next removed by transient transfection of Flp-recombinase. Three color fluorescence in situ hybridization (FISH) revealed that translocations occurred relatively frequently, with 20 of 100 screened cells harboring a split of the *FOSB* bracketing probes (chromosome 19) and a colocalization of the distal *FOSB* probe to the *SERPINE1* (chromosome 7) (supplementary figure 6.1b). hiPSC clones derived from single cells were screened by PCR

and the presence of the *SERPINE1-FOSB* gene fusion was confirmed in 2 out of 73 (2.7% of targeted cells, clones D3 and G6) (figure 6.1b). Sanger sequencing of PCR products confirmed the correct translocation (figure 6.1a and supplementary figure 6.2a). This shows that although translocations between chromosomes 7 and 19 were relatively common events (20% of targeted cells showed translocation detected by FISH), most of these translocations likely occur via non-homologous end joining (NHEJ) and possibly contain large deletions/insertions. They were therefore not detected during PCR screening, resulting in only 2 correctly targeted clones (2.7% targeting efficiency). The targeted allele of hiPSC clone D3 was found to have an FRT remaining between *SERPINE1* and *FOSB* as expected (figure 6.1a), while this insert was absent in the targeted allele of hiPSC clone G6 due to the translocation occurring via NHEJ (supplementary figure 6.2a). The non-targeted wild-type alleles of *SERPINE1* and *FOSB* were also Sanger sequenced. In clone D3 a single nucleotide insertion was found in both the non-targeted wild-type *SERPINE1* intron 1 and the non-targeted wild-type *FOSB* intron 1 (supplementary figure 6.2b,c). In clone G6, a 9 base-pair deletion was found in the non-targeted wild-type *FOSB* intron 1 (supplementary figure 6.2b). In addition, clone G6 contained an insertion of ∼1220 bp of the repair template in the non-targeted wild-type *SERPINE1* intron 1, which was evident on the DNA gel and Sanger sequencing (figure 6.1b and supplementary figure 6.2c). Analysis of the corresponding cDNA showed presence of fused *SERPINE1* 5' UTR and *FOSB* exon 2 in both clones D3 and G6 (supplementary figure 6.2d) identical to that found in PHE patients, and the presence of correctly spliced wild-type *SERPINE1* (supplementary figure 6.2e). Neither clone D3 or G6 had other karyotypic abnormalities, other than the balanced t(7;19)(q22;q13) translocation, as seen using COmbined Binary RAtio Labeling Fluorescence in Situ Hybridization (COBRA-FISH) (figure 6.1c).

To verify that the targeting with CRISPR/Cas9 did not result in deleterious off-target effects, whole-genome sequencing was performed. No additional copy number variations, insertions or deletions, structural variants or single nucleotide variants (SNVs) were found in the coding genome of the targeted hiPSC clones D3 and G6 ($\text{hiPSC}^{SERPINE1\text{-}FOSB}$) compared to the parental control hiPSCs (hiPSC^{WT}) (figure 6.1d). Furthermore, the in silico predicted off target sites for the guide-RNAs used showed no additional alterations (synonymous or non-synonymous) compared with the untargeted parental control hiPSCs (figure 6.1d). To verify pluripotency of the targeted and parental control hiPSC lines, teratoma assay was performed in mice. Targeted and parental control hiPSCs retained the ability to form tissues derived from all three germ layers (endoderm, mesoderm and ectoderm), showing that CRISPR-Cas9 targeting has not affected pluripotency (figure 6.1e).

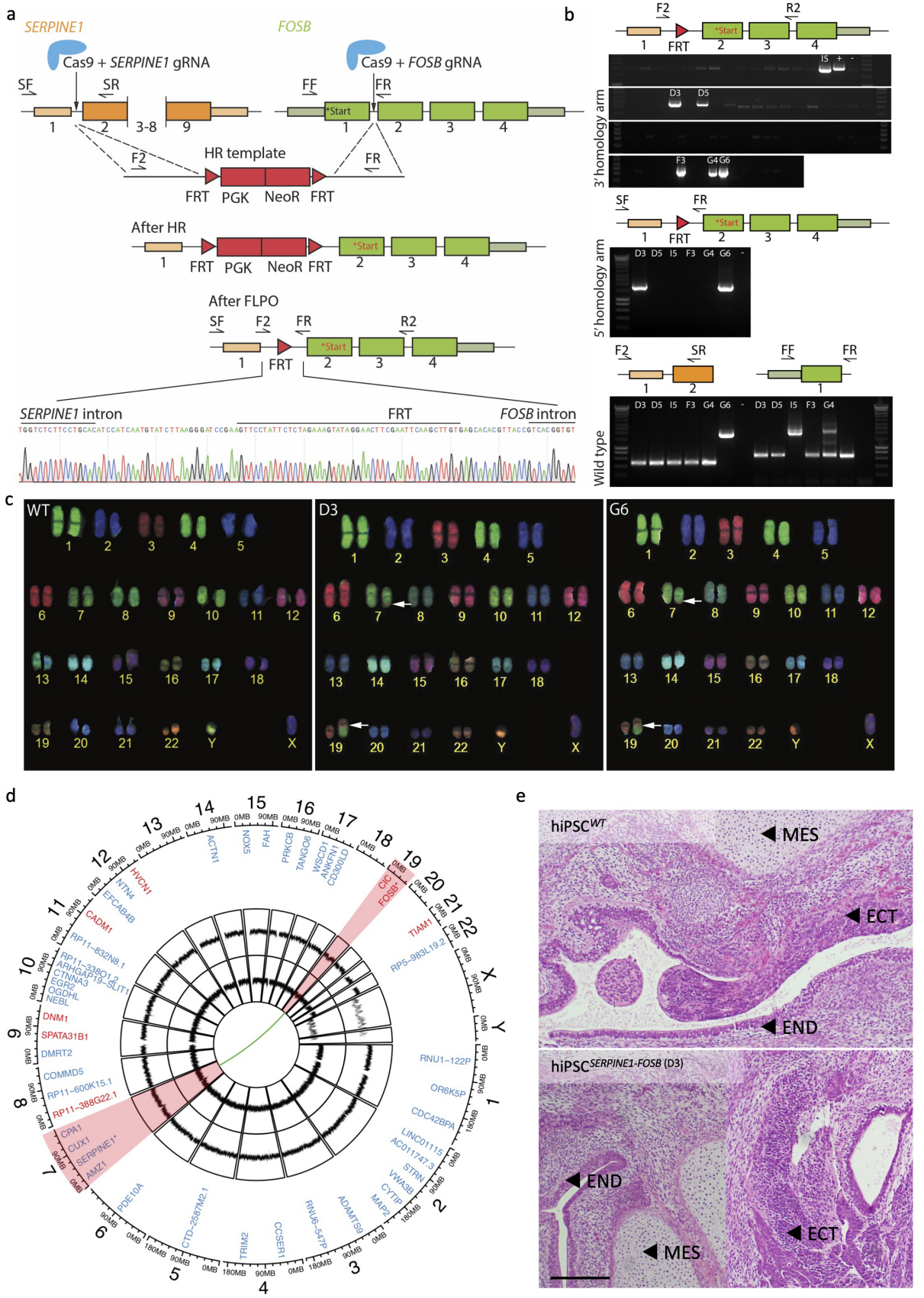

Figure 6.1: Caption on next page.

Figure 6.1: Generation and characterization of hiPSCs with a *SERPINE-FOSB* fusion. (a) Schematic overview of the targeting strategy for generation of a *SERPINE1-FOSB* gene fusion. Filled boxes are exons, lines introns. *FOSB* start codons are labeled in the figure, in black text represents the original start codon while the new start codon after the fusion is shown in red. Two double stranded breaks were introduced in the genome guided by two gRNAs in *SERPINE1* intron 1 and *FOSB* intron 1. A repair template used for homologous recombination (HR template) with neomycin resistance cassette flanked by Flp-recombinase sequences (FRT), as well targeted genomic locus prior (After HR) and after FLP-mediated neomycin removal (after FLPO). Bottom panel shows Sanger sequencing of PCR products from the clone with translocation validating HDR recombination of *SERPINE1* and *FOSB* with remaining FRT sequence left from the repair template (D3 clone). (b) Representative results of PCR screen on single cell-derived hiPSC clones using primers (F2, R2 and SF, SR; F2, SR and FF and FR) shown in panel above the PCR screen results. Two targeted clones (D3 and G6) were identified out of 73 screened clones. PCR shows clone G6 has a large insert in the *SERPINE1* wild-type allele. (c) COBRA-FISH on colony metaphase cells of WT, D3 and G6 hiPSC clones shows a balanced translocation t(7;19)(q22;q13); furthermore no additional chromosomal abnormalities were evident in any of the screened cells. (d) Whole genome sequencing was performed and the results are summarized in a Circos plot. The first layer shows all genes that are potential off-target sites for the gRNA for *FOSB* (red) and *SERPINE1* (blue). No mutations were found in the off-target sites and the surrounding 100 bases. The second and third layers show Copy Number Analysis (CNA) for clones D3 and G6 respectively compared to the isogenic control. No Copy Number Variations (CNVs) are detected. The green connection line shows the detected *SERPINE1-FOSB* fusion, as detected in both clones D3 and G6. Chromosomes 7 and 19, involved in the translocation, are highlighted in red. (e) Teratoma formation in mice. Top panel shows teratomas formed from the hiPSC^{WT}, the bottom panel from the hiPSC$^{SERPINE1\text{-}FOSB(D3)}$; two sections of each are shown. Cellular derivatives of the three germ lineages are indicated: mesoderm (MES), ectoderm (ECT) and endoderm (END). Scale bar indicates 200 μm.

6.4.2 Differentiation and characterization of ECs from hiPSC^{WT} and hiPSC$^{SERPINE1\text{-}FOSB}$ lines

hiPSCs with and without *SERPINE1-FOSB* fusion were differentiated into ECs using a protocol previously described (15–17) (figure 6.2a). hiPSC-ECs were purified on day 10 of differentiation by CD31+ cell selection, expanded and cryopreserved for further characterization. hiPSC-ECs^{WT}and hiPSC-ECs$^{SERPINE1\text{-}FOSB}$ differentiated from two targeted clones (D3 and G6) exhibited typical EC morphology (figure 6.2b and data not shown) and showed cell surface expression of known EC markers, such as vascular endothelial (VE)-cadherin (VEC), CD31, CD34, VEGFR2, VEGFR3 and CD105, as expected and in accordance with our previous findings (16) (figure 6.2c,d and supplementary figure 6.3a,b). Interestingly, hiPSC-ECs derived from both the D3 and G6 targeted clones displayed increased expression of CD105 (figure 6.2d and supplementary figure 6.3b), which is known to be upregulated in tumor endothelial cells (34) as well as in vascular tumors (35). Moreover, expression of *FOSB* mRNA showed a 4.9 log2 fold increase in hiPSC-ECs from clone D3 and a 5.9 log2 fold increase in hiPSC-ECs from clone G6 compared to the isogenic hiPSC-ECs derived from parental non-targeted hiPSC line (figure 6.2e and supplementary figure 6.3c). The increase in *FOSB* expression at the mRNA level was also evident as an increase in protein expression by Western blot, where FOSB was detected in hiPSC-ECs$^{SERPINE1\text{-}FOSB}$ but not in hiPSC-ECs^{WT}(figure 6.2f and supplementary figure 6.3d).

6.4.3 Functionality of ECs from hiPSC^{WT} and hiPSC$^{SERPINE1\text{-}FOSB}$ lines

To investigate the effect of the *SERPINE1-FOSB* fusion on hiPSC-ECs functionality, we next preformed assessment of proliferation and Matrigel tube formation assay. *SERPINE1-FOSB* fusion caused increased EC proliferation. The effect measured after 24 hours was most prominent in basal EC growth medium supplemented with 1% platelet-poor serum (PPS) (1.9-fold increase), followed by basal EC growth medium supplemented with both 1% PPS and VEGF (1.58 vs 2.27-fold) (figure 6.2g). No significant differences in EC proliferation were observed using complete EC growth medium (full) that in addition to VEGF also contained bFGF, indicating that FOSB overexpression caused by the *SERPINE1-FOSB* fusion may result in a VEGF-independent growth advantage for ECs. Matrigel tube formation assays showed significant increase in number of junctions (147 vs 218, $p<0.001$) and meshes (53 vs 85, $p<0.005$) in hiPSC-ECs$^{SERPINE1\text{-}FOSB}$ compared to isogenic control hiPSCs-ECs^{WT} after 48 hours (figure 6.2h).

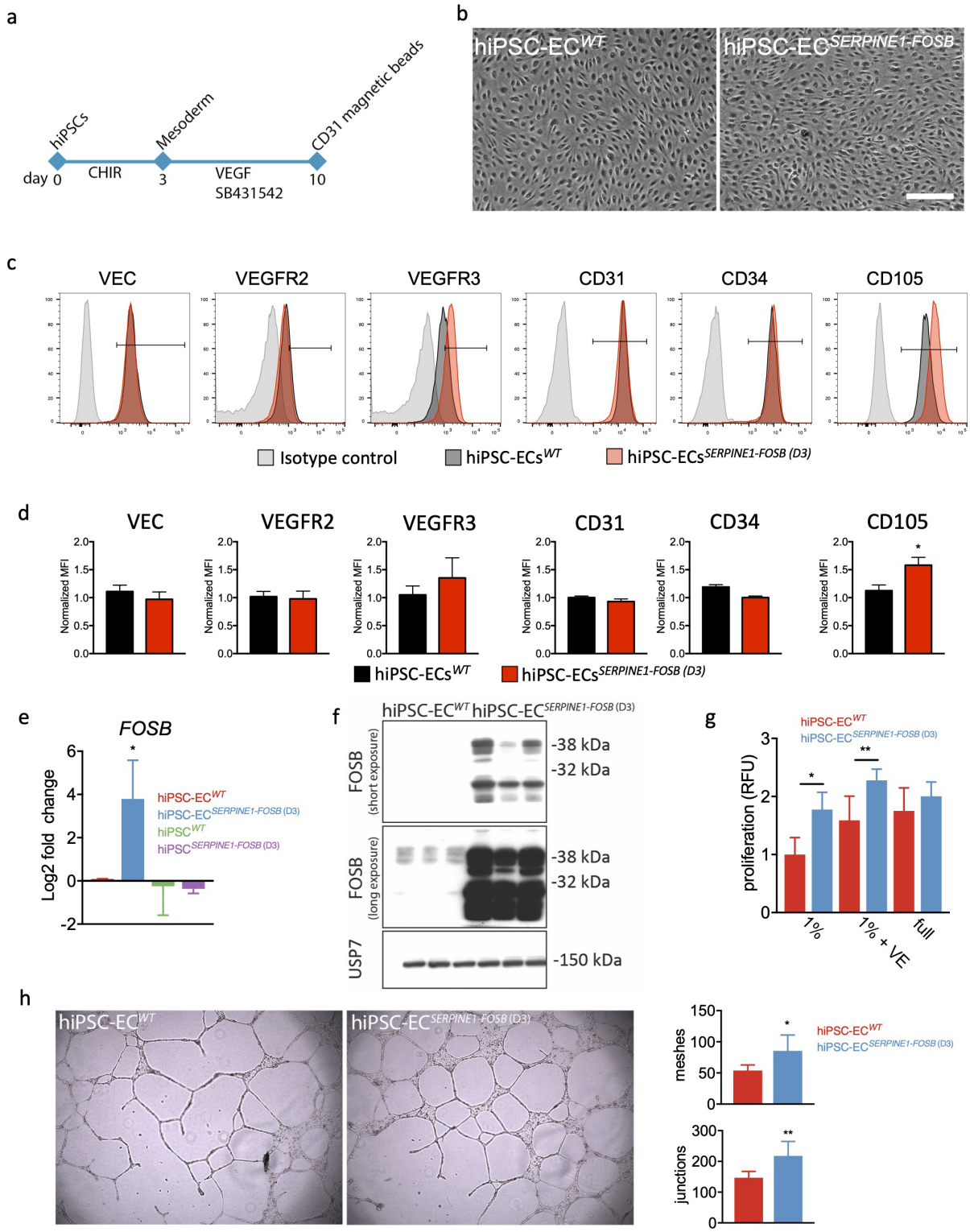

Figure 6.2: Caption on next page.

Figure 6.2: Differentiation and characterization of hiPSC-ECs with *SERPINE1-FOSB* fusion. (a) Schematic overview of the differentiation protocol and purification of ECs from hiPSCs. (b) Bright field images showing typical EC morphology of hiPSC-ECs. Scale bar represents 500 μm. (c) FACS analysis of EC markers expression on isolated ECs at passage 3 (P3) from hiPSC-ECs^{WT}(black filled histogram) and hiPSC-ECs$^{SERPINE1\text{-}FOSB(D3)}$ (red filled histogram), and relevant isotype control (gray filled histogram). (d) Quantification of normalized relative surface expression levels (MFI) of VEC, VEGFR2, VEGFR3, CD31, CD34 and CD105. Error bars are SD, * $p<0.005$. (e) Real-time qPCR analysis of FOSB expression in hiPSCs^{WT}, hiPSCs$^{SERPINE1\text{-}FOSB(D3)}$, hiPSC-ECs^{WT}and hiPSC-ECs$^{SERPINE1\text{-}FOSB(D3)}$. Expression is determined relative to hiPSC-ECs^{WT}, shown as log2 fold change. Error bars are SD, * $p<0.05$. (f) Western blot of FOSB expression in hiPSC-ECs^{WT} and hiPSC-ECs$^{SERPINE1\text{-}FOSB(D3)}$. Short and long exposure of the gel is shown. USP7 was used as a housekeeping control. (g) Analysis of hiPSC-ECs^{WT}and hiPSC-ECs$^{SERPINE1\text{-}FOSB(D3)}$ proliferation rates when cultured in basal endothelial cell growth medium supplemented with 1%PPS (1%), 1%PPS supplemented with 50 ng/ml VEGF (1% VE) or complete EC growth medium (full) for 24 hours. Proliferation was determined by using a Presto Blue assay. Error bars are shown as SD, * $p<0.0001$, ** $p<0.0005$. (h) Representative images of Matrigel tube formation assay using hiPSC-ECs^{WT}and hiPSC-ECs$^{SERPINE1\text{-}FOSB(D3)}$ at the 48h time point. Right panel shows quantification of the number of junctions and meshes. Error bars are SD, * $p<0.005$, ** $p<0.001$. All experiments were performed in triplicate using three independent batches of hiPSC-ECs.

6.4.4 Barrier function of ECs from hiPSC^{WT} and hiPSC$^{SERPINE1\text{-}FOSB}$ lines

Barrier function of hiPSC-ECs with and without the *SERPINE1-FOSB* fusion was next examined by real-time impedance spectroscopy with an integrated assay of electric wound healing, as demonstrated previously (15). The *SERPINE1-FOSB* fusion resulted in a significant decrease in barrier function of hiPSC-ECs (figure 6.3a,b and supplementary figure 6.4a,b). Barrier function depends on the integrity of cell junction complexes that form tight- and adherence junctions. Therefore, we also investigated junctional integrity in hiPSC-ECs with *SERPINE1-FOSB* fusion using the tight junctional marker zonula occludens (ZO)-1, the adherence junctional marker VEC and counterstained for F-actin (figure 6.3d). Presence of less organized "zig-zag" patterns of ZO1 and VEC was evident for hiPSC-ECs$^{SERPINE1\text{-}FOSB}$ compared to the hiPSC-ECs^{WT}(figure 6.3d). Which is in line with reduces barrier function of hiPSC-ECs with *SERPINE1-FOSB* fusion.

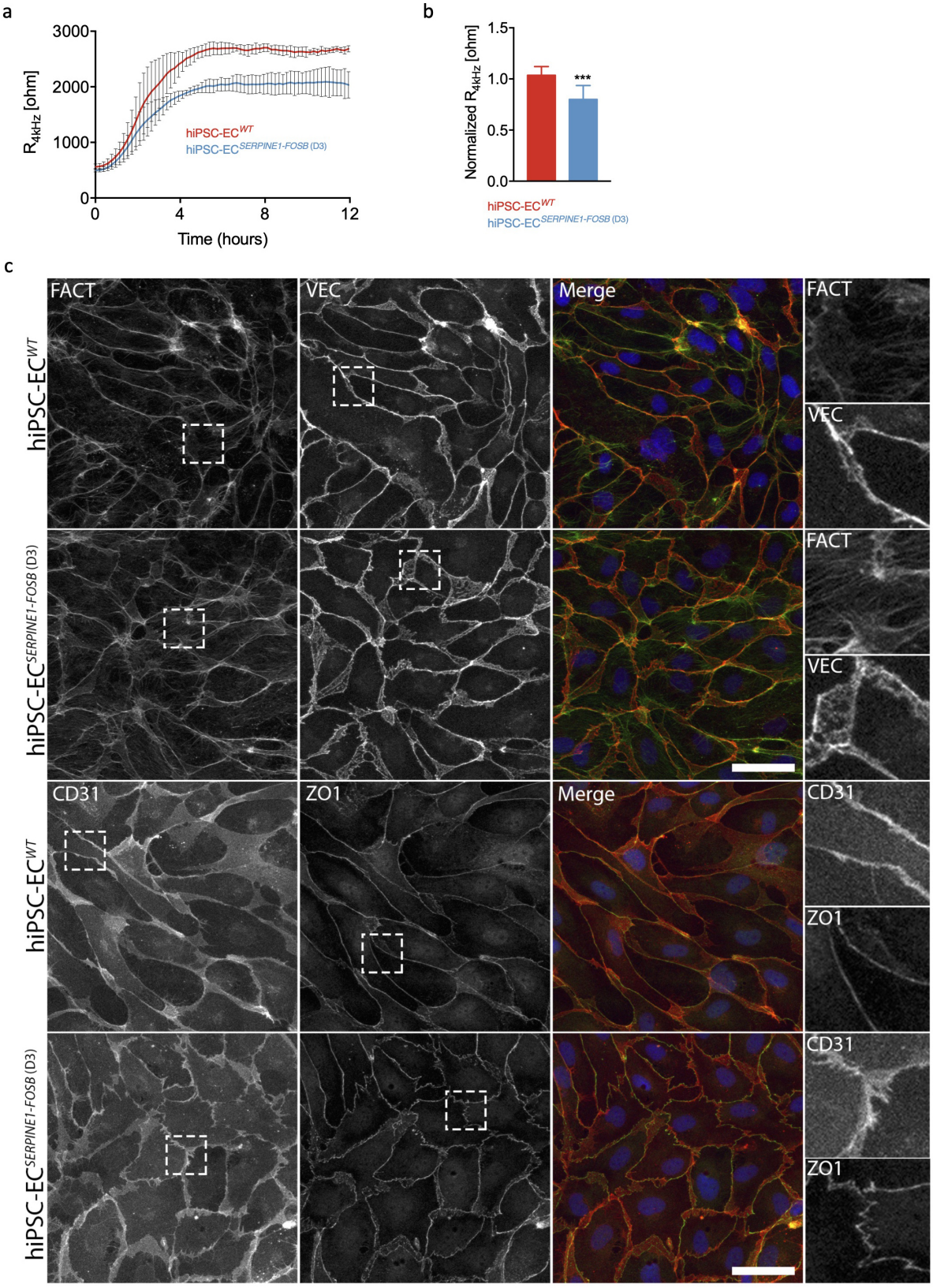

Figure 6.3: Caption on next page.

Figure 6.3: Assessment of barrier function of hiPSC-ECs with *SERPINE1-FOSB* fusion. (a) Representative absolute resistance of the EC monolayer in complete EC growth medium. Errors bars are shown as ±SD. (b) Normalized resistance [4 kHz] of the EC monolayer in complete EC growth medium. Error bars are shown as ±SD of six independent biological experiments. *** $p<0.001$. (c) Representative immunofluorescent images of FACT, VEC, CD31 and ZO1 to analyze the cell adherence and tight junctions. The top panels with merged images show FACT in green, VEC in red and DAPI in blue. The bottom panels with merged images show CD31 in red, ZO1 in green and DAPI in blue. The right panels show further enlarged areas selected from the shown images (dashed squares). Scale bar represents 50 μm. Experiments were performed in triplicate using three independent batches of hiPSC-ECs.

6.4.5 Functionality of hiPSC-ECs from hiPSC^{WT} and hiPSC$^{SERPINE1\text{-}FOSB}$ lines *in vivo* in mice

In order to test the functionality and the ability to form functional perfused blood vessels, hiPSC-ECs with and without *SERPINE-FOSB* translocation were injected in mice in a Matrigel Plug Assay that allows assessment of vasculogenesis, as described previously (15). Matrigel plugs were excised and analyzed 4- and 16-weeks post-transplantation. Both hiPSC-ECs^{WT}and hiPSC-ECs$^{SERPINE1\text{-}FOSB(D3)}$ formed stable vessels *in vivo* composed of human ECs evident at the 4-weeks (figure 6.4a) and 16-weeks post-transplantation (figure 6.4c). Quantification of the vessel density showed comparable areas covered by human vessels, demonstrating that both hiPSC-ECs^{WT}and hiPSC-ECs$^{SERPINE1\text{-}FOSB(D3)}$ had similar abilities to form vessels *in vivo* (figure 6.4b,d). The vessels were perfused (as indicated by the presence of red blood cells) (figure 6.4a,c). Moreover, FOSB positive ECs were evident in the Matrigel plugs with hiPSC-ECs$^{SERPINE1\text{-}FOSB(D3)}$, but not the Matrigel plugs with hiPSC-ECs^{WT}(figure 6.4e). Furthermore, FOSB positive hiPSC-ECs$^{SERPINE1\text{-}FOSB(D3)}$ also invaded the surrounding mouse soft tissues (the striated muscle) at 16-weeks post-transplantation in two of the three mice whereas this was not observed in any of the mice with hiPSC-ECs^{WT}transplants (figure 6.4f, and 6.4g).

The hiPSC-ECs$^{SERPINE1\text{-}FOSB(D3)}$ vessels at 16 weeks were disorganized and disarrayed and often contained thrombi (conglomeration of fibrin and platelets, containing red and white blood cells) (figure 6.4h,i). Thrombi were quantified using phosphotungstic acid-haematoxylin (PTAH) staining (thrombus positive vessels 20.67 vs 81.33 counted in 5.7 mm^2, n=3, p=0.1) (figure 6.5j).

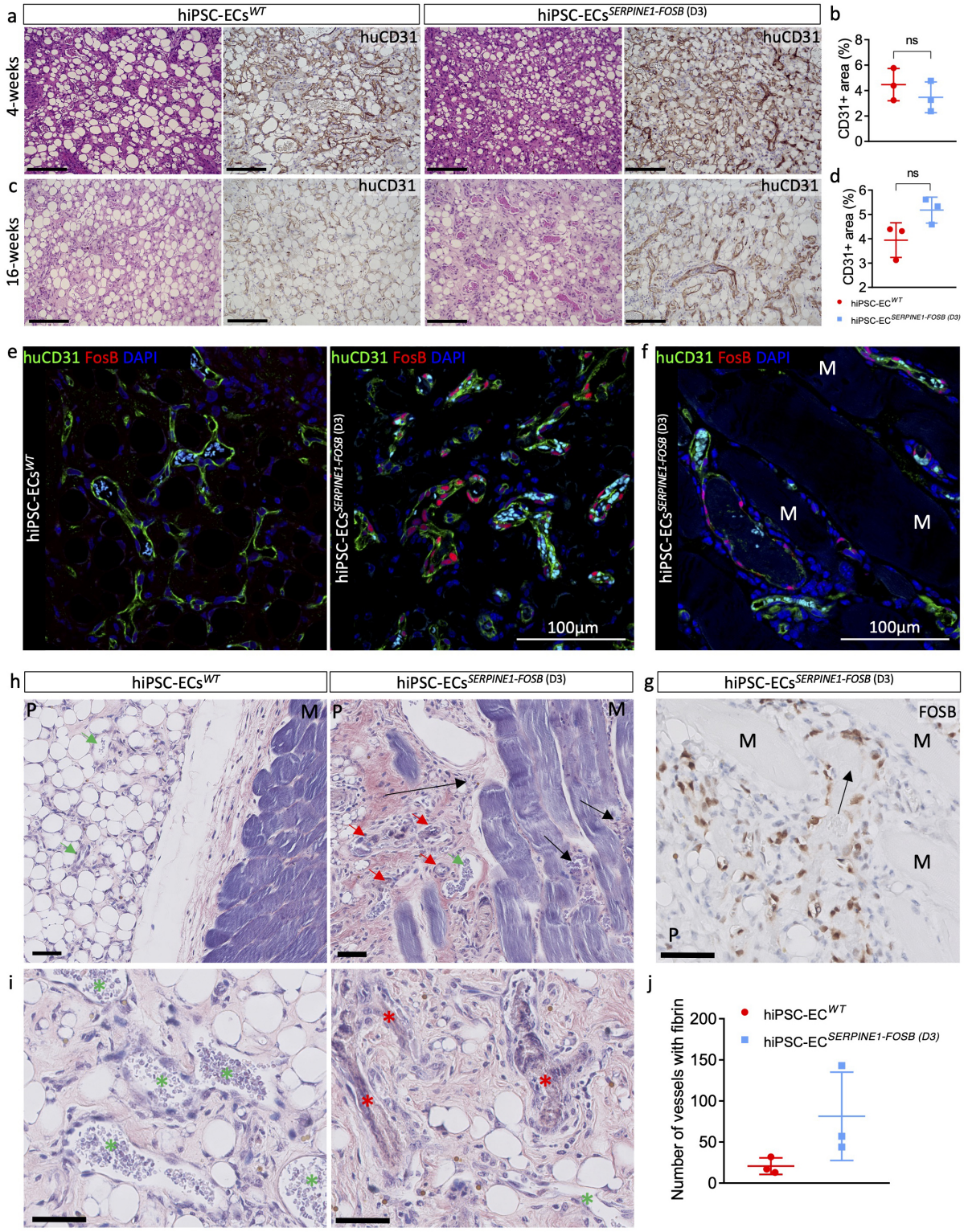

Figure 6.4: Caption on next page.

Figure 6.4: *In vivo* vasculogenesis assay for hiPSC-ECs^{WT}and hiPSC-ECs$^{SERPINE1\text{-}FOSB(D3)}$. (a,c) H&E and CD31 staining of FFPE tissue from the Matrigel plug harvested after 4- (shown in panel (a)) and 16- (shown in panel (c)) weeks. Both hiPSC^{WT} and hiPSC$^{SERPINE\text{-}FOSB(D3)}$ show vessel formation. Scale bar indicates 100 μm. (b,d) Vessel density was estimated by quantification of the human CD31+ area at 4- and 16-weeks. The 4- and 16-week timepoints showed no significant difference in human CD31+ area. (e,f) Double immunofluorescent staining with FOSB and human CD31 antibodies counterstained with DAPI on cryosections from Matrigel plug containing hiPSC-ECs^{WT}and hiPSC-ECs$^{SERPINE\text{-}FOSB(D3)}$. FOSB is shown in red, CD31 in green and DAPI is blue. The left panel shows the hiPSC-ECs^{WT}experiment, the right panel the hiPSC-ECs$^{SERPINE\text{-}FOSB(D3)}$ experiment. (g) FOSB IHC on FFPE tissue from Matrigel plug with hiPSCSERPINE-FOSB (D30) ECs. Scale bar 50 μm. Panels (f,g) show invasion of FOSB positive hiPSC-ECs$^{SERPINE1\text{-}FOSB(D3)}$ into the striated muscle at 16-weeks post-transplantation. Surrounding mouse muscle (indicated by M) and the matrigel plug (indicated by a P). (h,i) PTAH stained sections from the *in vivo* vasculogenesis assay. hiPSC-ECs^{WT}(left panel) and hiPSC-ECs$^{SERPINE\text{-}FOSB(D3)}$ (right panel) are shown. Both images show the surrounding mouse muscle (indicated by M) and the Matrigel plug (indicated by a P). Vessels with and without thrombi are indicated by red and green arrows, respectively (h) and red and green stars (i). The black arrows indicate areas with infiltration in the mouse muscle. The scale bar indicates 50 μm. (j) Quantification of vessels containing PTAH positive thrombi in hiPSC-ECs^{WT}and hiPSC-ECs$^{SERPINE\text{-}FOSB(D3)}$, in an area of 5.7 mm2, n=3 and p=0.1.

6.4.6 Transcriptome analysis of ECs from hiPSC^{WT} and hiPSC$^{SERPINE1\text{-}FOSB}$ lines

The transcriptomes of hiPSC-ECs with and without *SERPINE1-FOSB* fusion were compared. 630 and 592 differentially expressed genes (DEGs)(PFDR$\leq$0.05) were upregulated and downregulated respectively in hiPSC-ECs$^{SERPINE1\text{-}FOSB}$ compared to hiPSC-ECs^{WT}(figure 6.5a). Both *FOSB* and *SERPINE1* were significantly upregulated in hiPSC-ECs$^{SERPINE1\text{-}FOSB}$ compared to hiPSC-ECs^{WT}. Enrichment analysis using the KEGGs (Kyoto Encyclopedia of Genes and Genomes) pathway database revealed several signaling pathways significantly enriched in DEGs upregulated in hiPSC-ECs$^{SERPINE1\text{-}FOSB}$. These included focal adhesion, ECM-receptor interaction, Pathways in cancer, PI3K-Akt, MAPK, TGF-beta and HIF-1 signaling pathways, and Glycolysis/Gluconeogenesis (figure 6.5b and supplementary figure 6.5). Upregulation of glycolytic genes in hiPSC-ECs$^{SERPINE1\text{-}FOSB}$ (supplementary figure 6.5h) indicates possible changes in the metabolic state of ECs, as previously demonstrated for tumor ECs (36). No signaling pathways were significantly enriched in DEGs upregulated in hiPSC-EC^{WT}. Gene Ontology (GO) enrichment analysis revealed alterations in the following biological processes in hiPSC-ECs$^{SERPINE1\text{-}FOSB}$: extracellular matrix organization, angiogenesis, cell-matrix adhesion,

inflammatory response, cell junction organization, regulation of TGF-beta receptor signaling pathway and others (figure 6.5c). By contrast, response to interferon-gamma was the only biological process significantly enriched in DEGs upregulated in hiPSC-EC^{WT} (figure 6.5c). To demonstrate the relationship between the genes and identified GOs, a gene network map was next constructed using DEGs upregulated in hiPSC-ECs$^{SERPINE1\text{-}FOSB}$ (total of 182 genes) (figure 6.5d). Gene interaction analysis was next performed using Ingenuity pathway analysis (IPA). Gene interaction networks related to cancer, cellular movement and growth, and TGF-β signaling pathway were used to demonstrate interaction between the identified dysregulated genes and *FOSB* in hiPSC-ECs$^{SERPINE1\text{-}FOSB}$ (figure 6.5e). FOSB regulates *SERPINE1* directly, which is in line with our previous finding that truncated FOSB was able to regulate its own transcription (22), as well as via SMAD3. Both exhibit a self-regulatory mechanism, which could further activate many genes in the network of cellular growth and proliferation and cancer processes directly or indirectly through activation of the TGF-β signaling pathway (figure 6.5e).

6.5 Discussion

There is an urgent need for *in vitro* models to study rare translocation-driven tumors, both to identify the functional consequences of the translocation, and to identify potential therapeutic targets. We used CRISPR/Cas9 to induce a tumor-associated translocation in hiPSCs, specifically the *SERPINE1-FOSB* translocation in hiPSCs to model the rare vascular tumor PHE. Two hiPSC clones among 73 clones screened contained the translocation. In one of the clones (D3), the translocation was introduced via HDR using the donor DNA template, while in the second clone (G6) the translocation occurred via NHEJ. As the breakpoints were in intronic regions of the two involved genes, in both clones the transcribed and spliced RNA resulted in the typical *SERPINE1-FOSB* chimeric RNA. Other groups have also shown that CRISPR/Cas9 can be used to introduce chromosomal translocations in other cells, notably hMSCs via both NHEJ, but also via HDR using donor DNA templates and additional exposure to low doses of DNA-PKC inhibitor (NU7441) to block NHEJ (13). Although blocking NHEJ to increase HDR proved efficient in mouse embryonic stem cells (mESCs) and human cell lines (37), the efficiency of this approach remains debated in hiPSCs (38). Our results showed that both NHEJ and HDR pathways can be used to introduce translocations in hiPSCs. It would be interesting to investigate further whether the use of NHEJ inhibitors can indeed enhance the occurrence of translocations via HDR.

Whole genome sequencing of both parental and targeted hiPSC lines showed no deleterious structural variations, copy number variations or mutations at the predicted off-target

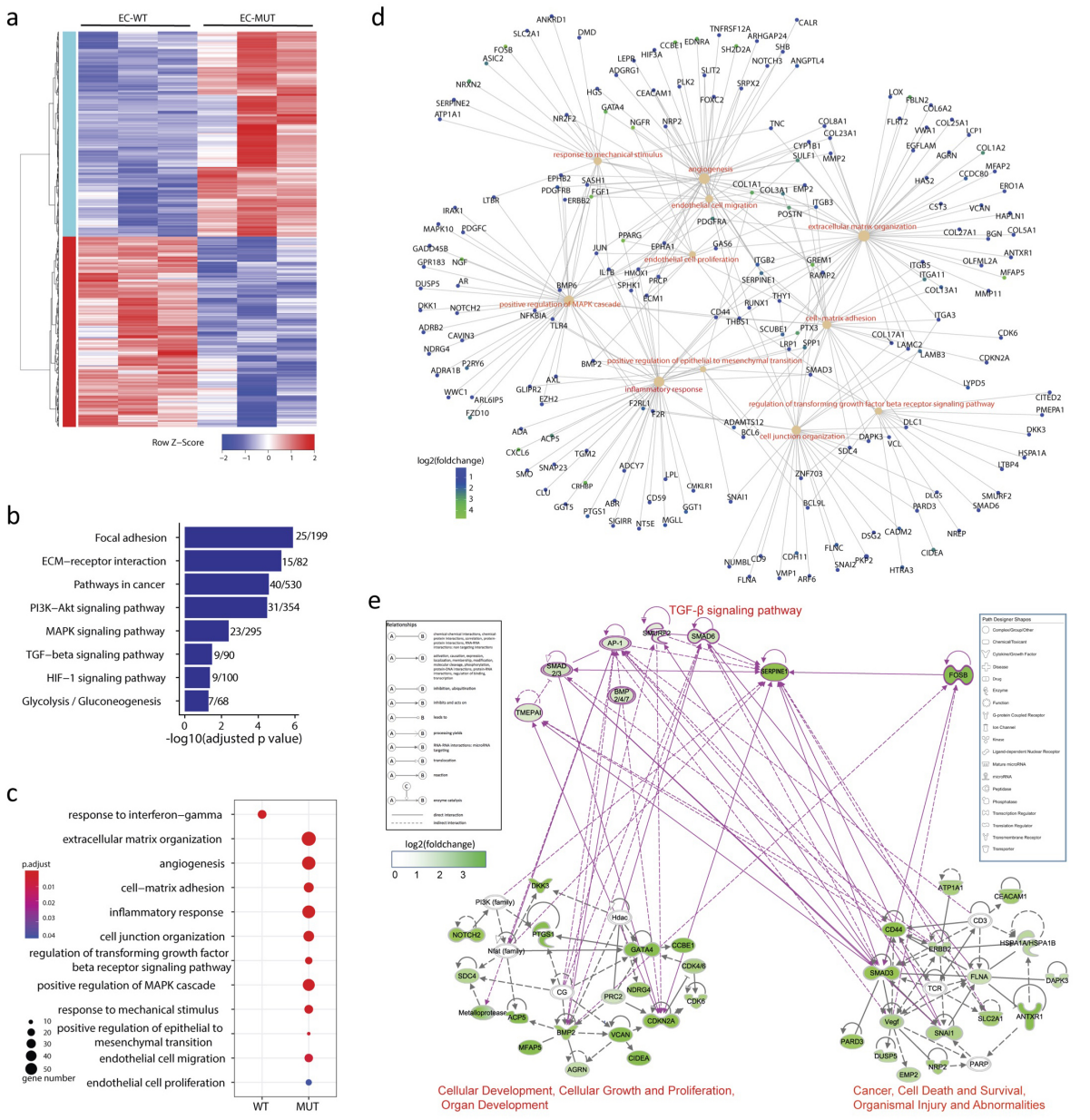

Figure 6.5: Transcriptome analysis of hiPSC-ECs with and without *SERPINE1-FOSB* translocation. (a) Hierarchical clustering analysis (HCA) of differentially expressed genes (DEGs) between hiPSC-ECs^{WT}(WT) and hiPSC-ECs$^{SERPINE1\text{-}FOSB(D3)}$ (MUT) samples. 630 and 592 significantly upregulated and downregulated genes in MUT were identified compared to WT ECs (PFDR$\leq$0.05). (b) Representative KEGG pathways enriched in upregulated DEGs in MUT ECs (-log10(adjusted p value)) and number of enriched genes within total genes of each pathway are shown. (c) Representative Gene ontologies (GOs) that enriched in downregulated (WT) and upregulated (MUT) DEGs. Size and color indicate gene number and adjusted p value of each GO. (d) Cnetplot of genes associated with enriched GOs (c), color indicates the log2(fold change) of gene expression in MUT compared to WT. (e) Gene interaction network constructed using all genes shown in (c) with Ingenuity pathway analysis (IPA). *SERPINE1*, *FOSB* were added manually. Interactions among *FOSB* and *TGF-β* signaling pathway and two networks were generated using IPA. Color indicates the log2(fold change) of gene expression in MUT compared to WT.

sites for the gRNAs. Any phenotypic changes observed were thus most likely associated with the *SERPINE1-FOSB* translocation.

We recently showed that overexpression of truncated FOSB in human umbilical vein ECs (HUVECs) recapitulated some features of PHE pathology (22). However, the drawback of overexpression is that they lack the regulatory elements for cell type-specific expression at levels found in tumor cells. Here we addressed the shortcomings of our original model by introducing the truncated protein under the endogenous *SERPINE1* regulatory elements via *SERPINE1-FOSB* fusion using CRISPR/Cas9-induced translocation in hiPSCs, thereby recreating the fusion with endogenous regulatory elements of *SERPINE1*. We found that the *SERPINE1-FOSB* fusion results in upregulation of FOSB expression specifically in ECs, and not in undifferentiated hiPSCs, in line with known high SERPINE1 expression in vascular cells and its function as a direct transcriptional target of the activator protein 1 (AP-1) family of proteins that includes FOSB (4, 39). Thus, we here show that self-regulation of its own promoter, and thereby of the expression of the fusion product that is considered the driver alteration in PHE, only occurs in endothelial cells and not in undifferentiated hiPSCs. These results indicate lineage restricted expression of the fusion and confirm that PHE should be considered a vascular tumor.

Vasculogenesis assays *in vivo* in mice in which hiPSC-ECs$^{SERPINE1\text{-}FOSB(D3)}$ or hiPSC-ECs^{WT}were co-injected with bone marrow stromal cells (BMSCs) supported our *in vitro* findings and showed most strikingly the infiltrative growth pattern reminiscent of human PHE (5). Vessels from hiPSC-ECs$^{SERPINE1\text{-}FOSB(D3)}$ were haphazardly arranged compared to hiPSC-ECs^{WT}and contained significantly higher numbers of fibrin thrombi, in two of three hiPSC-ECs$^{SERPINE1\text{-}FOSB(D3)}$. These results are in line with the *in vitro* barrier function analysis and suggest that the endothelium is aberrant inducing thrombi formation. However, some aspects of PHE were not recapitulated *in vivo*. The tumor cells typically do not form vessels in PHE but instead are spindle-shaped and co-express endothelial markers (CD31 and ERG) and keratin AE1AE3, features that are absent in our *in vivo* model. It might be that the 16 weeks time frame is not enough to develop these features in vivo. Invasion of hiPSC-ECs$^{SERPINE1\text{-}FOSB(D3)}$ into surrounding mouse soft tissue was observed at 16-weeks, but not at the 4-week time-point, which may suggest that the development of the phenotype takes time.

Transcriptome analysis of hiPSC-ECs with the fusion revealed differentially expressed genes associated with several pathways that are known to be related to cancer, such as TGF-beta signaling, adhesion, metabolism, inflammatory response, angiogenesis and endothelial cell migration. These are all linked to the phenotypes we observed in vitro and *in vivo* in our model, and recapitulate some aspects of PHE. Moreover, these pathways that we here identify to be regulated by the *SERPINE1-FOSB* fusion provide rationale

to develop targeted treatment strategies for inoperable multifocal PHE patients. In line with our previous report of a patient with a complete clinical remission following the multi-tyrosine kinase inhibitor telatinib, we confirm upregulated MAPK signaling and overexpression of PDGFRA and -B induced by the fusion in the current model. Moreover, we identify PI3K-Akt signaling which can be targeted using mTOR inhibitors. Indeed, anecdotal responses to mTOR inhibition in patients with PHE have been reported (40–42).

In summary, we showed that hiPSCs and hiPSC-ECs can be used to model fusion-driven tumors using CRISPR/Cas9 and a donor DNA template to introduce the translocation. The differentiated hiPSC-ECs carrying the pathognomonic translocation gave insights into the tumorigenesis of PHE, and elucidated the pathways regulated by the fusion product, that may provide rationale to develop targeted treatment strategies for inoperable multifocal PHE. Overall, this approach facilitated the elucidation of the role of specific fusion genes in the development of specific rare cancer subtypes for which cell lines are presently lacking.

Bibliography

[1] Mitelman F, Johansson B, Mertens F. The impact of translocations and gene fusions on cancer causation; 2007. Available from: `http://www.nature.com/articles/nrc2091`.

[2] Mertens F, Antonescu CR, Mitelman F. Gene fusions in soft tissue tumors: Recurrent and overlapping pathogenetic themes. Genes Chromosomes Cancer. 2016;55(4):291–310. doi:10.1002/gcc.22335.

[3] Trombetta D, Magnusson L, von Steyern FV, Hornick JL, Fletcher CDM, Mertens F. Translocation t(7;19)(q22;q13)-a recurrent chromosome aberration in pseudomyogenic hemangioendothelioma? Cancer Genetics. 2011;204(4):211–215. doi:10.1016/j.cancergen.2011.01.002.

[4] Walther C, Tayebwa J, Lilljebjorn H, Magnusson L, Nilsson J, von Steyern FV, et al. A novel SERPINE1-FOSB fusion gene results in transcriptional up-regulation of FOSB in pseudomyogenic haemangioendothelioma. J Pathol. 2014;232(5):534–540. doi:10.1002/path.4322.

[5] Hornick JL, Fletcher CD. Pseudomyogenic hemangioendothelioma: a distinctive, often multicentric tumor with indolent behavior. Am J Surg Pathol. 2011;35(2):190–201. doi:10.1097/PAS.0b013e3181ff0901.

[6] Hung YP, Fletcher CDM, Hornick JL. FOSB is a useful diagnostic marker for pseudomyogenic hemangioendothelioma. American Journal of Surgical Pathology. 2017;41(5):596–606. doi:10.1097/PAS.0000000000000795.

[7] Billings SD, Folpe AL, Weiss SW. Epithelioid Sarcoma-Like Hemangioendothelioma. The American journal of surgical pathology. 2003;27(1):48–57. doi:10.1097/PAS.0b013e31821caf1c.

[8] Ide YH, Tsukamoto Y, Ito T, Watanabe T, Nakagawa N, Haneda T, et al. Penile pseudomyogenic hemangioendothelioma/epithelioid sarcoma-like hemangioendothelioma with a novel pattern of SERPINE1-FOSB fusion detected by RT-PCR–report of a case. Pathol Res Pract. 2015;211(5):415–420. doi:10.1016/j.prp.2015.02.003.

[9] Sanchez-Rivera FJ, Jacks T. Applications of the CRISPR-Cas9 system in cancer biology. Nat Rev Cancer. 2015;15(7):387–395. doi:10.1038/nrc3950.

[10] Schneidawind C, Jeong J, Schneidawind D, Kim IS, Duque-Afonso J, Wong SHK, et al. MLL leukemia induction by t(9;11) chromosomal translocation in human hematopoietic stem cells using genome editing. Blood advances. 2018;2(8):832–845. doi:10.1182/bloodadvances.2017013748.

[11] Torres R, Martin MC, Garcia A, Cigudosa JC, Ramirez JC, Rodriguez-Perales S. Engineering human tumour-associated chromosomal translocations with the RNA-guided CRISPR-Cas9 system. Nat Commun. 2014;5:3964. doi:10.1038/ncomms4964.

[12] Torres-Ruiz R, Martinez-Lage M, Martin MC, Garcia A, Bueno C, Castaño J, et al. Efficient Recreation of t(11;22) EWSR1-FLI1+in Human Stem Cells Using CRISPR/Cas9. Stem Cell Reports. 2017;8(5):1408–1420. doi:10.1016/j.stemcr.2017.04.014.

[13] Vanoli F, Tomishima M, Feng W, Lamribet K, Babin L, Brunet E, et al. CRISPR-Cas9-guided oncogenic chromosomal translocations with conditional fusion protein expression in human mesenchymal cells. Proc Natl Acad Sci U S A. 2017;114(14):3696–3701. doi:10.1073/pnas.1700622114.

[14] Takahashi K, Tanabe K, Ohnuki M, Narita M, Ichisaka T, Tomoda K, et al. Induction of pluripotent stem cells from adult human fibroblasts by defined factors. Cell. 2007;131(5):861–872. doi:10.1016/j.cell.2007.11.019.

[15] Halaidych OV, Freund C, van den Hil F, Salvatori DCF, Riminucci M, Mummery CL, et al. Inflammatory Responses and Barrier Function of Endothelial Cells Derived from Human Induced Pluripotent Stem Cells. Stem Cell Reports. 2018;10(5):1642–1656. doi:10.1016/j.stemcr.2018.03.012.

[16] Orlova VV, Drabsch Y, Freund C, Petrus-Reurer S, Van Den Hil FE, Muenthaisong S, et al. Functionality of endothelial cells and pericytes from human pluripotent stem cells demonstrated in cultured vascular plexus and zebrafish xenografts. Arteriosclerosis, Thrombosis, and Vascular Biology. 2014;34(1):177–186. doi:10.1161/ATVBAHA.113.302598.

[17] Orlova VV, Van Den Hil FE, Petrus-Reurer S, Drabsch Y, Ten Dijke P, Mummery CL. Generation, expansion and functional analysis of endothelial cells and pericytes derived from human pluripotent stem cells. Nature Protocols. 2014;9(6):1514–1531. doi:10.1038/nprot.2014.102.

[18] Vidigal JA, Ventura A. Rapid and efficient one-step generation of paired gRNA CRISPR-Cas9 libraries. Nat Commun. 2015;6:8083. doi:10.1038/ncomms9083.

[19] Kranz A, Fu J, Duerschke K, Weidlich S, Naumann R, Stewart AF, et al. An improved Flp deleter mouse in C57Bl/6 based on Flpo recombinase. Genesis. 2010;48(8):512–520. doi:10.1002/dvg.20641.

[20] Rossi S, Szuhai K, Ijszenga M, Tanke HJ, Zanatta L, Sciot R, et al. EWSR1-CREB1 and EWSR1-ATF1 fusion genes in angiomatoid fibrous histiocytoma. Clinical Cancer Research. 2007;13(24):7322–7328. doi:10.1158/1078-0432.CCR-07-1744.

[21] van IJzendoorn DG, de Jong D, Romagosa C, Picci P, Benassi MS, Gambarotti M, et al. Fusion events lead to truncation of FOS in epithelioid hemangioma of bone. Genes Chromosomes Cancer. 2015;54(9):565–574. doi:10.1002/gcc.22269.

[22] van IJzendoorn DGP, Sleijfer S, Gelderblom H, Eskens FALM, van Leenders GJLH, Szuhai K, et al. Telatinib Is an Effective Targeted Therapy for Pseudomyogenic Hemangioendothelioma. Clinical Cancer Research. 2018;24(11):2678–2687. doi:10.1158/1078-0432.CCR-17-3512.

[23] Szuhai K, Tanke HJ. COBRA: Combined binary ratio labeling of nucleic-acid probes for multi-color fluorescence in situ hybridization karyotyping. Nature Protocols. 2006;1(1):264–275. doi:10.1038/nprot.2006.41.

[24] Van IJzendoorn DGP, Forghany Z, Liebelt F, Vertegaal AC, Jochemsen AG, Bovée JVMG, et al. Functional analyses of a human vascular tumor FOS variant identify a novel degradation mechanism and a link to tumorigenesis. Journal of Biological Chemistry. 2017;292(52):21282–21290. doi:10.1074/jbc.C117.815845.

[25] Salvatori DCF, Dorssers LCJ, Gillis AJM, Perretta G, van Agthoven T, Gomes Fernandes M, et al. The MicroRNA-371 Family as Plasma Biomarkers for Monitoring Undifferentiated and Potentially Malignant Human Pluripotent Stem Cells in Teratoma Assays. Stem Cell Reports. 2018;11(6):1493–1505. doi:10.1016/j.stemcr.2018.11.002.

[26] Sacchetti B, Funari A, Remoli C, Giannicola G, Kogler G, Liedtke S, et al. No Identical "Mesenchymal Stem Cells" at Different Times and Sites: Human Committed Progenitors of Distinct Origin and Differentiation Potential Are Incorporated as Adventitial Cells in Microvessels. Stem Cell Reports. 2016;6(6):897–913. doi:10.1016/j.stemcr.2016.05.011.

[27] Wu TD, Nacu S. Fast and SNP-tolerant detection of complex variants and splicing in short reads. Bioinformatics (Oxford, England). 2010;26(7):873–81. doi:10.1093/bioinformatics/btq057.

[28] Wu TD, Watanabe CK. GMAP: a genomic mapping and alignment program for mRNA and EST sequences. Bioinformatics. 2005;21(9):1859–1875. doi:10.1093/bioinformatics/bti310.

[29] Hansen KD, Irizarry RA, WU Z. Removing technical variability in RNA-seq data using conditional quantile normalization. Biostatistics. 2012;13(2):204–216. doi:10.1093/biostatistics/kxr054.

[30] Robinson MD, McCarthy DJ, Smyth GK. edgeR: a Bioconductor package for differential expression analysis of digital gene expression data. Bioinformatics (Oxford, England). 2010;26(1):139–40. doi:10.1093/bioinformatics/btp616.

[31] Chen EY, Tan CM, Kou Y, Duan Q, Wang Z, Meirelles G, et al. Enrichr: interactive and collaborative HTML5 gene list enrichment analysis tool. BMC Bioinformatics. 2013;14(1):128. doi:10.1186/1471-2105-14-128.

[32] Kuleshov MV, Jones MR, Rouillard AD, Fernandez NF, Duan Q, Wang Z, et al. Enrichr: a comprehensive gene set enrichment analysis web server 2016 update. Nucleic acids research. 2016;44(W1):W90–7. doi:10.1093/nar/gkw377.

[33] Yu G, Wang LG, Han Y, He QY. clusterProfiler: an R package for comparing biological themes among gene clusters. Omics : a journal of integrative biology. 2012;16(5):284–7. doi:10.1089/omi.2011.0118.

[34] Miller DW, Graulich W, Karges B, Stahl S, Ernst M, Ramaswamy A, et al. Elevated expression of endoglin, a component of the TGF-?-receptor complex, correlates with proliferation of tumor endothelial cells. International Journal of Cancer. 1999;81(4):568–572. doi:10.1002/(SICI)1097-0215(19990517)81:4<568::AID-IJC11>3.0.CO;2-X.

[35] Verbeke SL, Bertoni F, Bacchini P, Oosting J, Sciot R, Krenacs T, et al. Active TGF-beta signaling and decreased expression of PTEN separates angiosarcoma of bone from its soft tissue counterpart. Mod Pathol. 2013;26(9):1211–1221. doi:10.1038/modpathol.2013.56.

[36] Cantelmo AR, Conradi LC, Brajic A, Goveia J, Kalucka J, Pircher A, et al. Inhibition of the Glycolytic Activator PFKFB3 in Endothelium Induces Tumor Vessel Normalization, Impairs Metastasis, and Improves Chemotherapy. Cancer Cell. 2016;30(6):968–985. doi:10.1016/j.ccell.2016.10.006.

[37] Komor AC, Badran AH, Liu DR. CRISPR-Based Technologies for the Manipulation of Eukaryotic Genomes. Cell. 2017;168(1-2):20–36. doi:10.1016/j.cell.2016.10.044.

[38] Chu VT, Weber T, Wefers B, Wurst W, Sander S, Rajewsky K, et al. Increasing the efficiency of homology-directed repair for CRISPR-Cas9-induced precise gene editing in mammalian cells. Nat Biotechnol. 2015;33(5):543–548. doi:10.1038/nbt.3198.

[39] Milde-Langosch K. The Fos family of transcription factors and their role in tumourigenesis. European Journal of Cancer. 2005;41(16):2449–2461. doi:10.1016/j.ejca.2005.08.008.

[40] Gabor KM, Sapi Z, Tiszlavicz LG, Fige A, Bereczki C, Bartyik K. Sirolimus therapy in the treatment of pseudomyogenic hemangioendothelioma. Pediatr Blood Cancer. 2018;65(2). doi:10.1002/pbc.26781.

[41] Joseph J, Wang WL, Patnana M, Ramesh N, Benjamin R, Patel S, et al. Cytotoxic and targeted therapy for treatment of pseudomyogenic hemangioendothelioma. Clin Sarcoma Res. 2015;5:22. doi:10.1186/s13569-015-0037-8.

[42] Ozeki M, Nozawa A, Kanda K, Hori T, Nagano A, Shimada A, et al. Everolimus for Treatment of Pseudomyogenic Hemangioendothelioma. J Pediatr Hematol Oncol. 2017;39(6):e328–e331. doi:10.1097/MPH.0000000000000778.

6.A Additional Figures

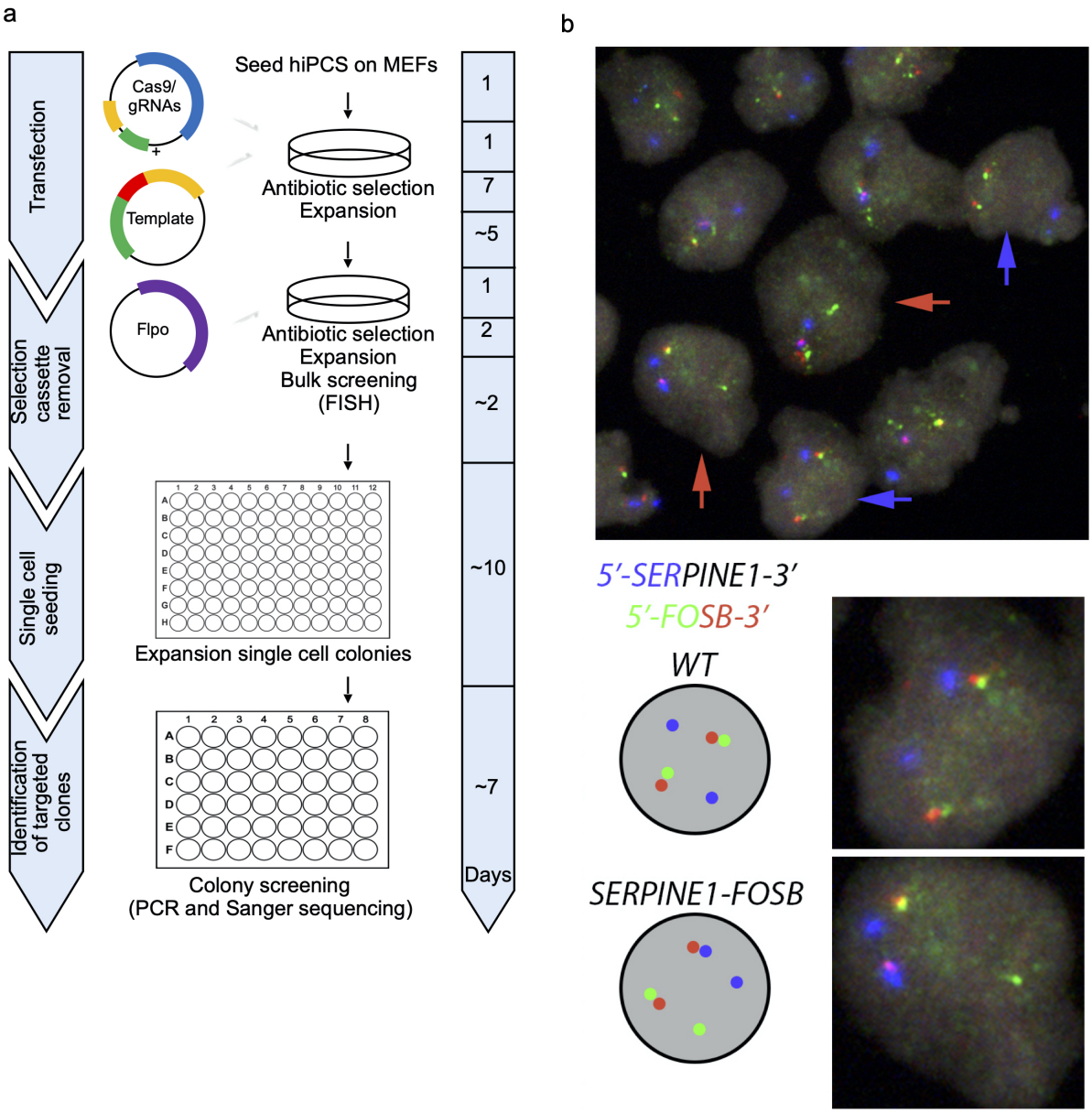

Additional Figure 6.1: Generation and characterization of hiPSCs with a *SERPINE-FOSB* fusion. (a) Schematic overview of the targeting and screening experimental workflow. (b) Three color FISH (Blue at 5' side of *SERPINE1*; green at 5' side of *FOSB* and red at 3' side of *FOSB*) for the detection of *SERPINE1-FOSB* fusion on hiPSC "bulk" culture prior to single-cell deposition. Red arrows indicate cells with the fusion, and blue arrows show wild-type cells. The right image shows a schematic and representative overview of targeted and wild-type cells, as detected with three color FISH.

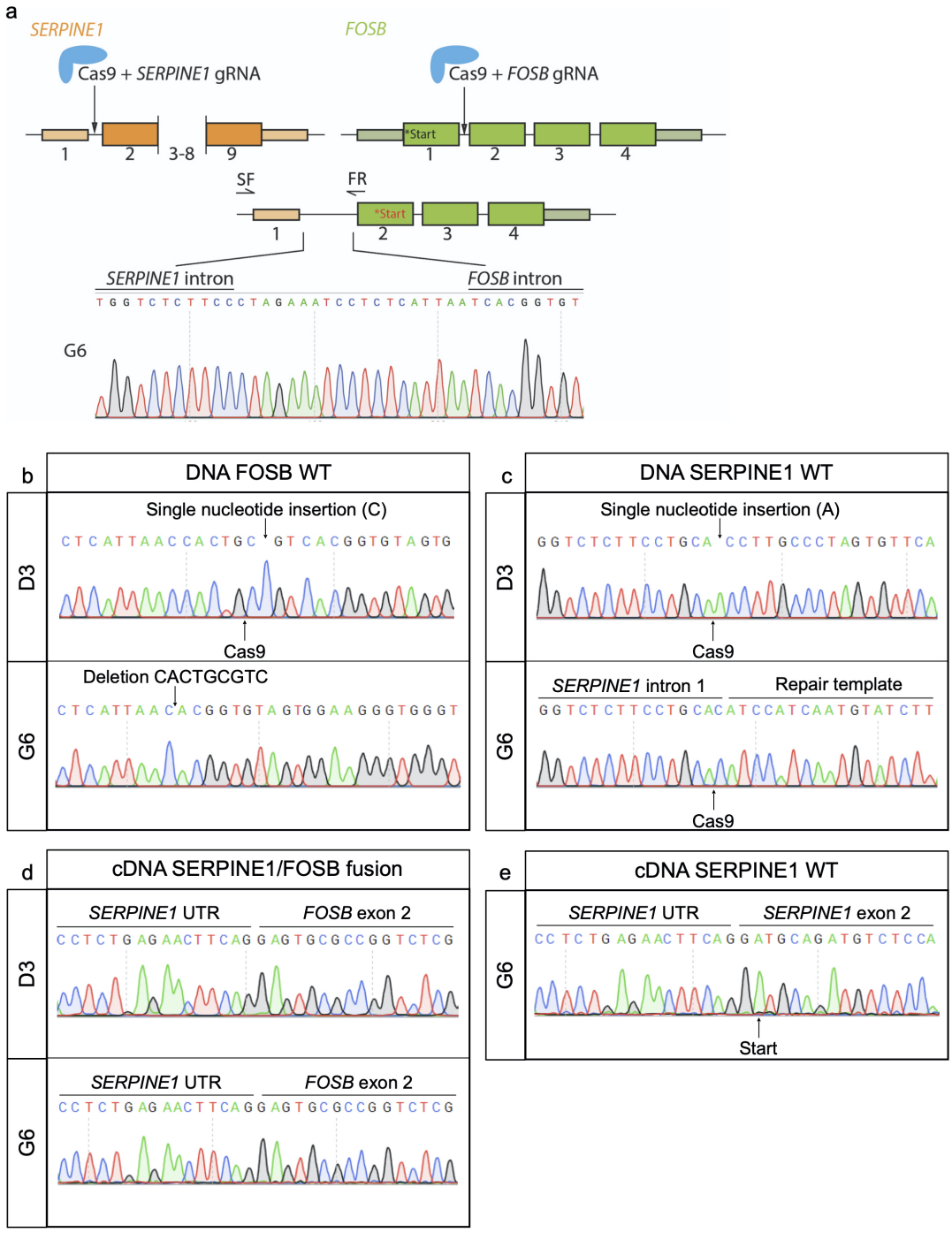

Additional Figure 6.2: Sanger sequencing of hiPSCs with a *SERPINE-FOSB* fusion. (a) Upper panel: schematic overview of NHEJ-mediated repair resulting in generation of clone G6. Bottom panel: Sanger sequencing of PCR products from G6 clone validating NHEJ recombination of *SERPINE1* and *FOSB* with a random piece of DNA inserted in the intron between the fusion. (b,c) Sanger sequencing of the non-targeted wild-type *FOSB* intron 1 and wild-type *SERPINE1* intron 1 in hiPSC clones D3 and G6. (d) Sanger sequencing of cDNA from clones D3 and G6 showing normal splicing of fusion *SERPINE1-FOSB* mRNA using forward primer on the *SERPINE1* UTR and a reverse primer on *FOSB* exon 3. (e) Sanger sequencing of the non-targeted wild-type *SERPINE1* cDNA with primers on the *SERPINE1* UTR and exon 2 showing that the insertion of the selection cassette fragment had no effect on splicing of *SERPINE1* mRNA in colony G6.

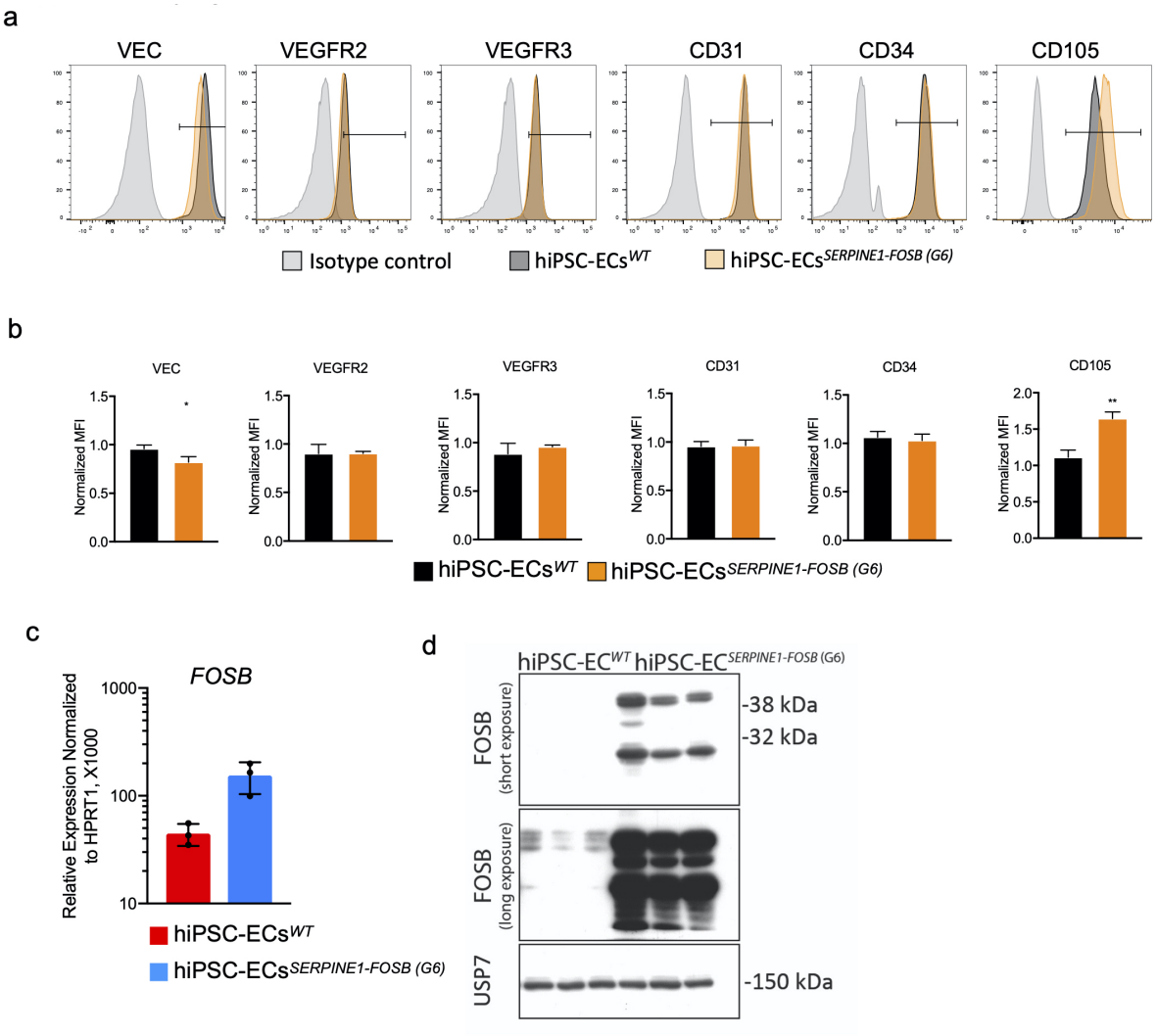

Additional Figure 6.3: Characterization of hiPSC-ECs with *SERPINE1-FOSB* fusion. (a) FACS analysis of EC markers expression on isolated hiPSC-ECs^{WT} (black filled histogram) and hiPSC-ECs$^{SERPINE\text{-}FOSB(G6)}$ (orange filled histogram) at passage 2 (P2) and relevant isotype control (gray filled histogram). (b) Quantification of relative surface expression levels (MFI) of VEC, VEGFR2, VEGFR3, CD31, CD34 and CD105. Experiments were performed in triplicate with three independent batches of hiPSC-ECs. Error bars are SD. (c) Real-time qPCR analysis of *FOSB* expression in hiPSCs^{WT}, hiPSCs^{G6}, hiPSCs, hiPSC-ECs^{WT} and hiPSC-ECs$^{SERPINE\text{-}FOSB(G6)}$. Experiments were performed with three independent batches of hiPSC-ECs. Expression is determined relative to hiPSC-ECs^{WT}, shown as log2 fold change. Error bars are SD. * $p<0.005$. (d) Western blot analysis of FOSB expression in hiPSC-ECs^{WT} and hiPSC-ECs$^{SERPINE\text{-}FOSB(G6)}$. USP7 was used as a housekeeping control.

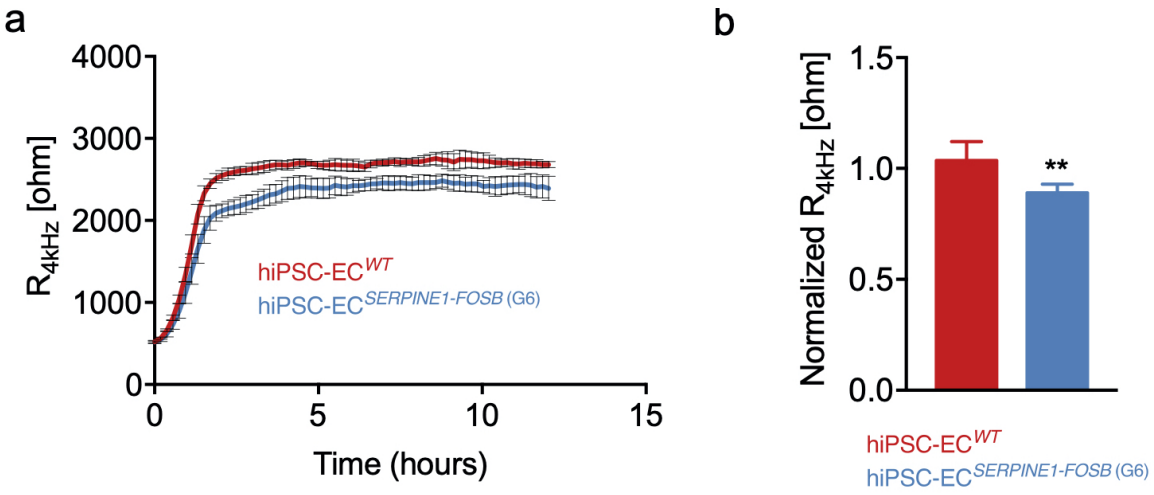

Additional Figure 6.4: Assessment of barrier function of hiPSC-ECs with *SERPINE1-FOSB* fusion. (a) Representative absolute resistance of the hiPSC-EC monolayer in complete EC growth medium. Errors bars are shown as ±SD. (b) Normalized resistance [4 kHz] of the hiPSC-EC monolayer in complete EC growth medium. Error bars are shown as ±SD of six independent biological experiments. *** $p<0.001$. Experiments were performed in triplicate using three independent batches of hiPSC-ECs.

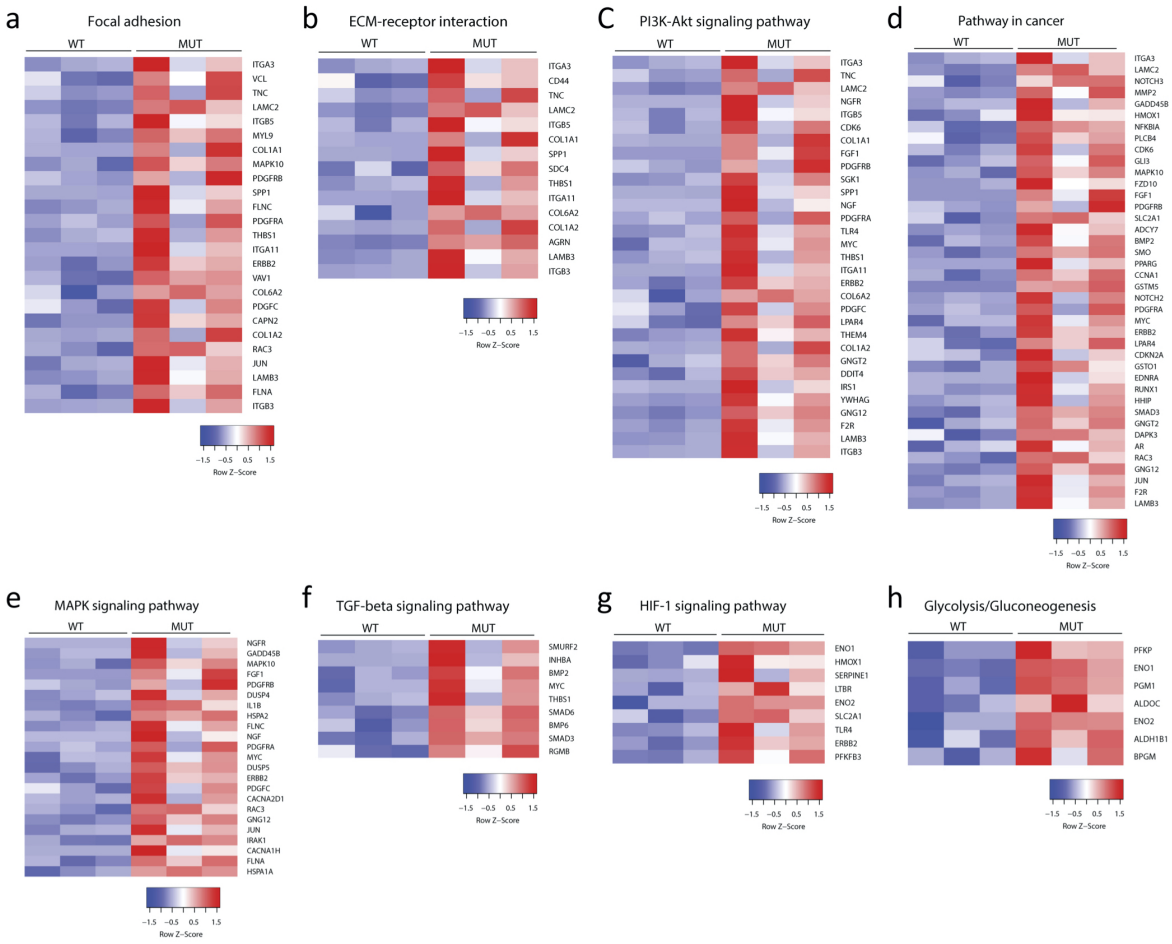

Additional Figure 6.5: KEGG pathways identified in hiPSC-ECsSERPINE1-FOSB (D3) upregulated DEGs. (a-h) Heatmaps of genes from eight representative KEGG pathways enriched in hiPSC-ECs$^{SERPINE\text{-}FOSB(D3)}$ upregulated DEGs.